TRANSACTIONS ON ELECTROMAGNETIC SPECTRUM

Rapid in-field processing of telluric electric field frequency selection method (TEFSM) data and its practical applications

Maoyue Zhu[1*], Tianchun Yang[1], Yawar Hussain[2] Qin Qin[1]

[1]School of Earth Sciences and Spatial Information Engineering, Hunan University of Science and Technology, 411201 Xiangtan, China

[2]Earth Science Department, Research Centre for Geological Risks-CERI, University of Rome “Sapienza”, Rome, Italy

*** Corresponding author e-mail address:** zmy18711314380@163.com

Received: 6 May 2026
Revised: 20 June 2026
Accepted: 25 June 2026

Research Article
Vol. 5 / No. 2 / 2026
Doi: 10.65819/tes.2026.v5i2.71

Abstract: The telluric electric field frequency selection method (TEFSM) is an electromagnetic exploration technique that utilizes the telluric electric field and the static effects to image the subsurface electrical structures. Currently, research on TEFSM has primarily focused on instrument development and practical applications, while theoretical algorithms have received limited attention. As a result, the interpretation of field data remains highly dependent on the quality of measurements and subjective judgment based on individual experience. In this paper, we propose an in-field signal processing approach to enhance anomaly resolution. The method involves logarithmic normalization of the measured data by dividing each value by the minimum data point in the logarithmic domain, thereby amplifying weak signals and improving contrast. Firstly, we applied this approach to process the data generated by a theoretical forward model. Subsequently, we validated its effectiveness through two field cases of groundwater prospecting—conducted in quartz sand-stone and granite areas—and one case of seepage detection at a reservoir. The applications show improved drilling success rates by enabling high-resolution delineation of target subsurface geological structures. Moreover, logarithmic normalization effectively high-lights potential leakage zones in the reservoir. The proposed approach is efficient, rapid, and cost-effective for groundwater exploration and related subsurface investigations.

Keywords: Frequency selection method, Signal processing approach, Groundwater, Seepage, Magnetotellurics

Cite this paper as: Zhu, M., Yang, T., Hussain, Y., Qin, Q. Rapid in-field processing of telluric electric field frequency selection method (TEFSM) data and its practical applications. Transactions on Electromagnetic Spectrum. 2026; 5(2): 35-50, Doi:10.65819/tes.2026.v5i2.71

1. INTRODUCTION

The principle of telluric electric field frequency selection method (TEFSM) is analogous to that of natural electromagnetic methods, such as magnetotellurics (MT) and audio magnetotellurics (AMT), in that both rely on naturally occurring electromagnetic fields to infer subsurface electrical resistivity structures [1-4]. However, TEFSM just utilizes a telluric electric field to study the underground electrical distribution [5]. Moreover, the static effect affecting MT and AMT’s interpretation is a useful signal in the TEFSM [6-8]. The TEFSM uses audio-frequency data (12 Hz-5000 Hz), and can obtain observed data quickly [9-12]. Considering the characteristics of this method, it has become a powerful tool in groundwater exploration and mine water disaster studies [6, 7, 13-15]. Although other geophysical methods can also be used for groundwater exploration, their cost is much higher than TEFSM [16, 17].

In 1976, Binghe Liang proposed using the natural electric pulse method and applied it to geological prospecting. Subsequently, many similar methods have been proposed by Chinese researchers, such as the sound frequency geoelectric field method ([18]), audio earth potential method ([19]), natural low-frequency electric field method ([20]), frequency selection method (FSM) of telluric current ([21]), geoelectric FSM, audio-frequency telluric electricity method ([22]), natural alternating field method ([23]), etc. Considering the similar theory and measuring methodology, these methods belong to the TEFSM family. With advancements in equipment, modern sensors are now capable of measuring multiple frequencies (exceeding 50), in contrast to the original single-frequency instruments. Additionally, their operational capabilities also evolved from purely mechanical to intelligent operations. These scholars' research on TEFSM has promoted the prosperity and development of this method, and the frequency selector has been applied to more than 100 countries in the world at present [24-26].

Although the TEFSM has made significant progress in recent years ([25-27]), field data interpretation is typically performed by analyzing raw measured data without preprocessing, leading to pseudo-sections with relatively low signal-to-noise ratios. This study proposes a logarithmic normalization signal processing method to improve the resolution and effectiveness of signals. The developed algorithm is validated using two field data case of groundwater exploration in Lengshuijiang City and Taojiang County, as well as a case of reservoir seepage detection in Xiangjiang New District, Hunan Province, China.

2. BASIC THEORY OF FREQUENCY SELECTION METHOD

The MT, AMT or controlled source audio-frequency magnetotellurics (CSAMT) methods are usually plagued by the static shift at present [28-31]. The static shifts caused by small-scale non-uniform bodies near the ground surface. This is because of the charge accumulation at the boundaries, which is seen as a significant spurious anomaly in the pseudo section, referred to as the "noodles phenomenon" [13]. As the static shift often affects the interpretation of results in these electromagnetic methods, it is suppressed by a certain method, such as impedance tensor decomposition, electromagnetic joint inversion, inversion with static shift and phase tensor method (e.g., [32-35]). Due to the use of high-frequency signals in TEFSM and its exploration depth usually within ca.300 m, the static shift is a useful signal for this method [6, 13].

According to the electromagnetic theory, if the electric field in the layered medium is polarized in the horizontal direction, the induced current flows in the same direction. If there is a shallow local inhomogeneous body in the background model, the electric current in the horizontal direction would be changed due to the local inhomogeneous body, and the charge would accumulate near the ground surface of the local inhomogeneous body. This accumulation of these charges results in a decrease or increase in electric field components measured at the ground surface [36-38].

At the interface between the anomaly and the surrounding medium, the normal components of electric displacement (D_n) is discontinuous, and it is calculated by the following formula.

$$D_{n1}-D_{n2}=q_s \tag{1}$$

where D_{n1} and D_{n2} are the normal components of electric displacement on both sides of the interface. The subscripts 1 and 2 represent different medium, n represents the normal component; q_s for the charge density on the surface of the object. Where $D=\varepsilon E$, E is the electric field. ε is the permittivity of space. We assume that the it is a scalar, and $\varepsilon \perp \varepsilon_0$, ε_0 is the permittivity of free space, then the follow formula can be obtain

$$E_{n1}\text{-}E_{n2} = q_s/\varepsilon_0 \tag{2}$$

The current density vector ($\boldsymbol{J}$) and electric field strength vector ($\boldsymbol{E}$) satisfies the following equation in the frequency domain as $\boldsymbol{J}=(\sigma-\mathrm{i}\varepsilon_0\omega)\boldsymbol{E}$, where σ is electrical conductivity, i is the imaginary unit, and $i^2=1$, ω is the angular frequency. Assuming the time dependence is $e^{-i\omega t}$. The continuity of normal component of the current density for AC situations can be described as follows:

$$(\sigma_1 - i\varepsilon_0\omega)E_{n1} = (\sigma_2 - i\varepsilon_0\omega)E_{n2} \tag{3}$$

By substituting equations (2) into (3), we can obtain

$$q_s = \varepsilon_0 E_{n2}\,\frac{\sigma_2 - \sigma_1}{\sigma_1 - i\varepsilon_0\omega} = \varepsilon_0 E_{n1}\,\frac{\sigma_2 - \sigma_1}{\sigma_2 - i\varepsilon_0\omega} \tag{4}$$

Due to $\sigma \gg \varepsilon_0\omega$ at the low frequency condition, the displacement current neglected, equation (4) can be simplified as:

$$q_s = \varepsilon_0 E_{n2}\,\frac{\sigma_2 - \sigma_1}{\sigma_1} = \varepsilon_0 E_{n1}\,\frac{\sigma_2 - \sigma_1}{\sigma_2} \tag{5}$$

Formula (5) indicates that the density of accumulated charge (q_s) is independent on frequency. Although q_s is very small, but it cannot be ignored. Because it will cause the general macro-effect on the electric field. Ward and Hohman ([39]) gave the expression of secondary field E_s generated by the accumulated charge as follows:

$$E_S = -\nabla\phi = -\nabla\int \frac{q_s}{4\pi\varepsilon_0\left|\mathbf{r}\right|}ds \tag{6}$$

where Φ is static potential, d_s is an area element with distributed charges, and $\boldsymbol{r}$ is the distance vector between the observation point and d_s. Equation 6 shows that the secondary field E_s has a positive relationship with the primary field. If the skin depth of EM waves is much larger than the size of the anomalous body, the electric field E_s can be detected. This shows that small 2D or 3D abnormal bodies at or near the earth's surface may have an impact on the whole electric field detection, leading to the static effect. The static effect in the observation over shallow anomalous bodies is quite apparent, and it is a valuable signal of TEFSM [6, 8, 13].

3. SIGNAL PROCESSING APPROACH AND FORWARD MODELING DATA PROCESSING

3.1 Processing Method

In comparison with MT or GPR ([40-44]), there are much lesser signal processing workflows and inversion strategies available for data processing in TEFSM, mainly attributed to the limitation in multi-component data recording.

Some attempts have been made in the literature to process such single-component results of TEFSM in recent years. Liu proposed the use of polynomial fitting for curve smoothing. Zhang proposed to use the stable background field values to normalize TEFSM data. However, the empirical evidence indicated the difficulties in determining the order and the number of points as required by the polynomial fitting formula, while the normalization process is complicated by the requirements that the profile curves should be complete and the background values are chosen in the areas which are less affected by the anthropogenic sources. In fact, the target application sites are usually in urban areas where the field sources are very complex and affected by diurnal variations as well. Under these circumstances, polynomial and normalization strategies are not very practical. Although the TEFSM has been successfully applied in the shallow groundwater exploration ([5]), the resolution of the signal is low in some cases, especially in the areas where there exists a weak contract between the conductivity of the medium and surrounding rock.

In practical situations, the observed data in TEFSM lie in a range between $n \times 10^{-2}$ and $n \times 10^{2}$ mV. This range can have interferences from cultural noise which is high in residential areas. To minimize these influences from noise sources, the present study proposed a logarithmic processing approach, which is based on the characteristic of observed data and can potentially improve the resolution of the signal. Logarithmic processing is an important tool that is often used to compress the range of signals in statistics, finance, physics, biology, among other disciplines. As in the field of experimental physics, data can be analyzed and modeled easily after underwent through logarithmic processing, and the accuracy and reliability of data can also be improved.

As in the case of TEFSM, the observed data sometimes have values less than 1 mV, if such data is logarithmic, it would be negative values. To solve this problem, we proposed the following formula.

$$P = \log(\Delta V / \Delta V_{\min}) \tag{7}$$

where ΔV is observed value, ΔV_{min} is the minimum of observed values on the profile, and P is the result of logarithmic processing. Equation (7) serves to compress the dynamic range of the dataset—specifically, by suppressing high-amplitude anomalies and enhancing low-amplitude ones. Consequently, logarithmic normalization reduces the disparity among variable magnitudes, improves distribution balance, effectively mitigates noise, and enhances model robustness. Moreover, in practical applications where the minimum potential difference, ΔV_{min}, equals 0 mV, division-by zero errors must be avoided. In such cases, ΔV_{min} is set to 0.001 mV.

3.2 Forward Modeling Data Processing

The two-dimensional (2D) model illustrated in Fig. 1(a) was simulated using the finite element method with bilinear interpolation over rectangular elements; the computational mesh comprises 200 × 100 nodes. All three electrical anomalies in Fig. 1(a) possess identical geometric dimensions. Under transverse magnetic (TM) polarization, the horizontal electric field component (E_x) at the Earth's surface was computed on a uniform grid with 5-m spacing in both the x- and z-directions, across 109 logarithmically spaced frequencies (f = 10^(1:0.025:3.7) Hz). The resulting profile curves and pseudo-section of E_x are presented in Fig. 1(b) and Fig. 1(d), respectively [45]. For clarity, only nine representative frequency profiles are shown in Fig. 1(b). As evident from Fig. 1(b) and Fig. 1(d), at identical burial depths, the anomaly intensity associated with the low-resistivity body is markedly stronger than that of the high-resistivity body. Furthermore, increasing the burial depth of the low-resistivity body leads to a pronounced attenuation of the anomalous signal [45].

The logarithmically normalized results shown in Fig. 1(b) and 1(d) are presented in Fig. 1(c) and 1(e), respectively. Logarithmic transformation enhances weak-signal anomalies: for instance, the relative anomaly amplitude of the 10 Hz profile curve in Fig. 1(c) is markedly more distinct than that in Fig. 1(b). Moreover, contour intervals in the simulated cross-section become uniform (Fig. 1(e)), reflecting a substantial reduction in the dynamic range of the data.

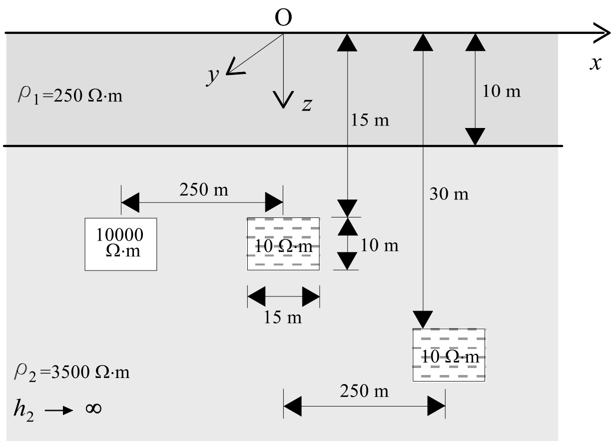

(a)

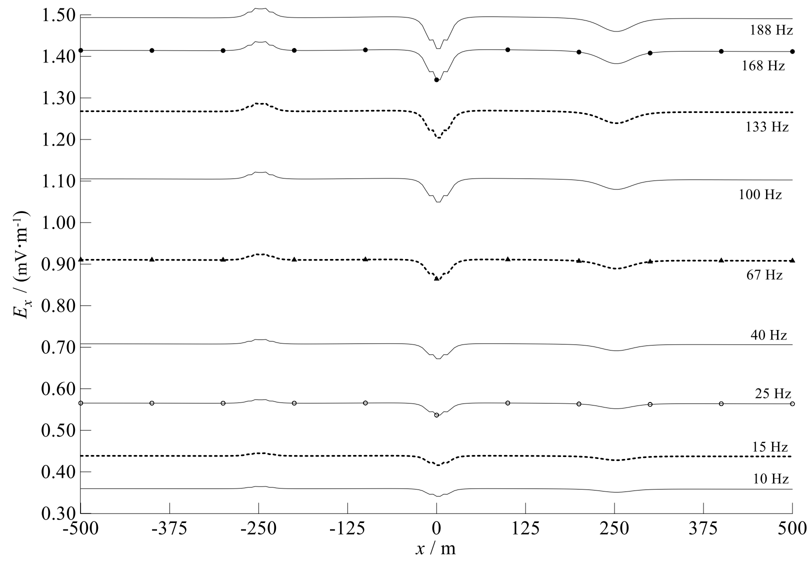

(b)

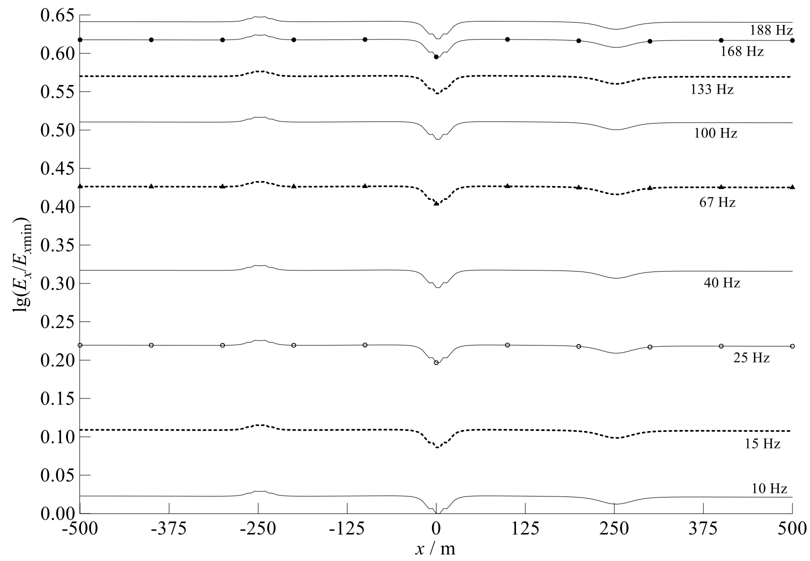

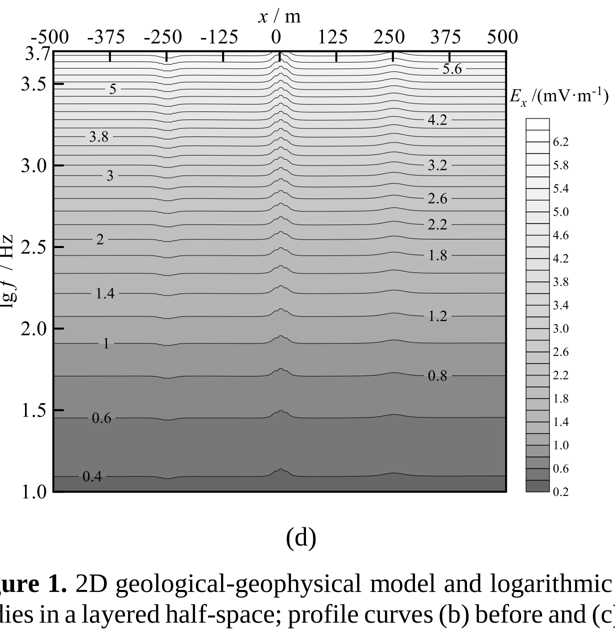

(c)

(d)

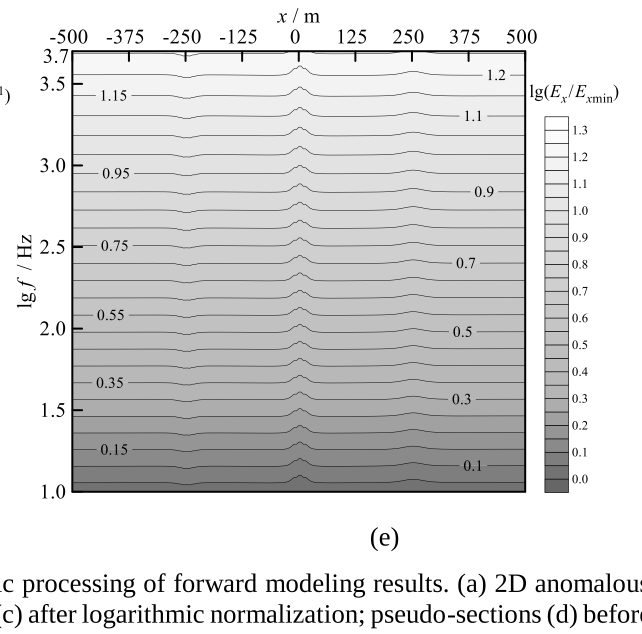

(e)

Figure 1. 2D geological-geophysical model and logarithmic processing of forward modeling results. (a) 2D anomalous bodies in a layered half-space; profile curves (b) before and (c) after logarithmic normalization; pseudo-sections (d) before and (e) after logarithmic normalization.

4. CASE STUDIES

The proposed signal processing scheme is applied to the two cases of groundwater exploration with TEFSM in different geological settings (i.e. quartz sandstone and caledonian granodiorite), and another case is seepage detection of a reservoir dam.

4.1 Groundwater Exploration in a Quartz Sandstone area

TEFSM has been adopted for the groundwater prospecting in the outcropped quartz sandstone with buried local patches of carbonaceous shale within geographic location (27º39'27.02"N and 111º29'54.38"E) in a factory of Lengshuijiang City (see Fig. 2). A TC300 equipment (see Fig. 3(a)) was used for data acquisition, and observation frequencies are 170 Hz, 67 Hz and 25 Hz. The electrode spacing (MN) and station intervals are 10 m and 5 m, respectively.

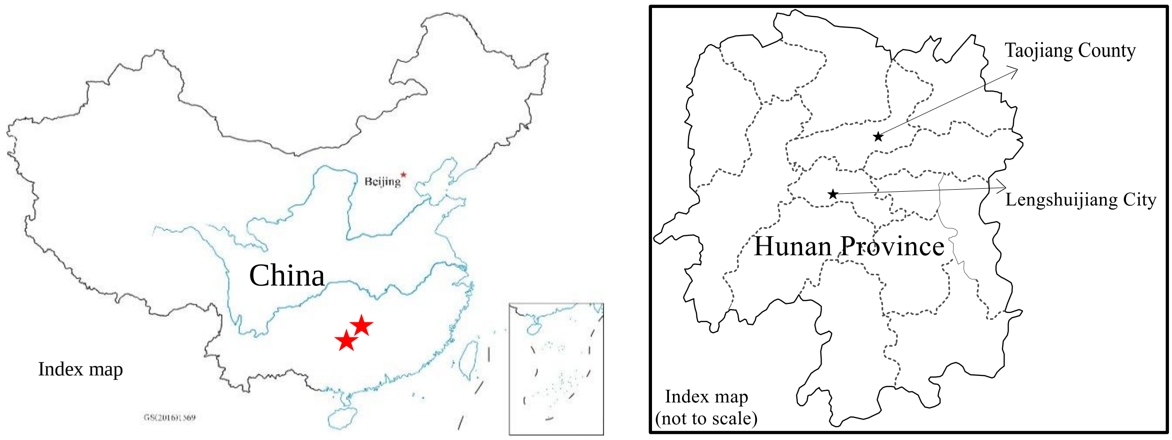

(a) (b)

Figure 2. (a) The locations of TEFSM application sites in Hunan Province in China. (b) The two black stars represent the studied locations.

The weight of the TC300 frequency selector host is only about 0.7 kg, which is very portable. In field applications using frequency-selective instruments, measurements are susceptible to diurnal variations and electromagnetic (EM) interference from the surrounding environment. However, because acquisition over a finite-length profile typically requires only a short time window, the influence of diurnal variation is generally negligible. Empirical evidence accumulated over nearly five decades of practical deployment indicates that repeated surveys along the same line at different times yield reliable results—provided the overall shape of the profile curve remains consistent. Anthropogenic EM interference poses a significant challenge to TEFSM measurements, as it does for all EM methods. In highly interfered areas, TEFSM surveys can only keep away from obvious interference sources or manually excluding spurious anomalies induced by noise. Notably, TEFSM employs hardware-based frequency selection and operates entirely in the frequency domain, unlike MT and AMT methods, which acquire full waveforms in the time domain. Consequently, TEFSM exhibits superior immunity to external interference compared with MT and AMT.

(a) (b)

Figure 3. (a) TC300 frequency equipment. (b) Photo of field measurement in Lengshuijiang City.

Figure 3(b) is a photo of field measurement in Lengshuijiang City, and the site is rather narrow because it lies in a small factory. The curve characteristics of the measured data with three frequencies are shown in Fig. 4. There is a septic tank near 120 m, cables and optical cables near 145 m, cables near 160 m, and a kitchen ventilator and monitoring equipment near 150 m on the profile. The above low-value anomalies which may associated with human activity are represented as cross marks in Fig. 4.

The anomalies at 40 m and 80 m on the profile as shown in Fig. 4 as black dots are further studied with multifrequency observed data. The number of sampling frequencies is 40, and the electrode spacing (*MN*) and the station interval are 10 m and 2 m, respectively. Fig. 5 and Fig. 6 show the results of groundwater detection conducted by the TC300 frequency selector near 40 m and 80 m along the profile. Figure 5(a) and Fig. 6(a) are profile curves of potential difference ΔV pre-processed, Fig. 5(b) and Fig. 6(b) are post-processed. Fig. 5(c) and Fig. 6(c) show the pseudo-sections of potential difference ΔV with 40 frequencies. The vertical axis is the apparent depth (h_s) obtained approximately by the skin depth formula of electromagnetic waves in Fig. 5(c), Fig. 5(d), Fig. 6(c) and Fig. 6(d). The inversion of apparent depth from skin depth is primarily grounded in empirical evidence derived from multiple drilling verification results obtained in prior field applications. However, variations in survey location, geological lithology, and other site-specific conditions inevitably introduce uncertainties and reduce the accuracy of the estimated apparent depth.

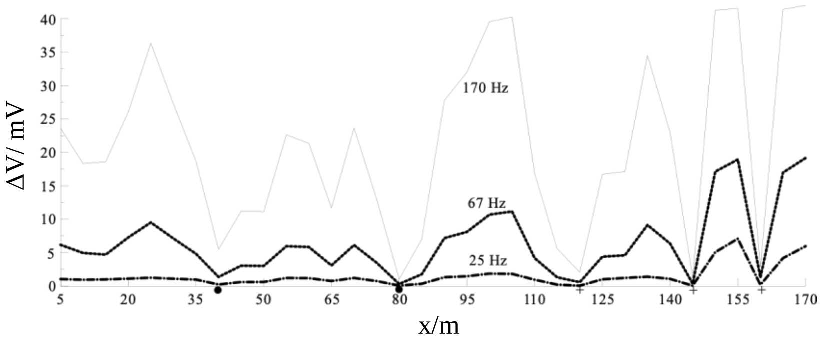

Figure 4. The exploration results using a triple frequency section in TEFSM for the profile in Lengshuijiang city. The black dot and cross indicate the abnormal positions, the potential sites for the groundwater exploration.

It can be seen from Fig. 5(a) that the synchronization of different frequencies' profile curves is good, and the abnormal range of relatively low potential lies in the range of 35～41 m on the profile. The lowest point of the anomaly is located at 36 m, which may be the best location for well drilling. After logarithmic processing, high values are suppressed and low values are raised, but the horizontal position of the anomaly center has not changed (see Fig. 5(b)).

A comparison between Fig. 5(a) and Fig. 5(b) reveals that the amplitude ratio of the low-impedance relative anomaly at 36 m—before and after logarithmic processing—changes from 1:32 to approximately 1.5:3.1. Similarly, the amplitude ratio of the relatively low-potential anomaly at 80 m in the profile shown in Fig. 6(a) shifts from ~3:28 to ~2.2:3.0 in Fig. 6(b). The synchronization of the curves in Fig. 6(a) is slightly worse than in Fig. 5(a), and the center of the low-value anomaly is less clear. The anomalous center at 80 m of the profile seems to become clearer after logarithmic processing (see Fig. 6(b)).

It can be seen from Fig. 5(c) and Fig. 6(c) that the "noodles phenomenon" occurs near the 36th m and the 80th m along the profile [6, 12, 13]. The static shift leads to the appearance of large areas of low potential in the pseudo-sections, and the center position of the static shift is unclear. Meanwhile, the conductivity characteristics of the near-surface medium are not distinguished.

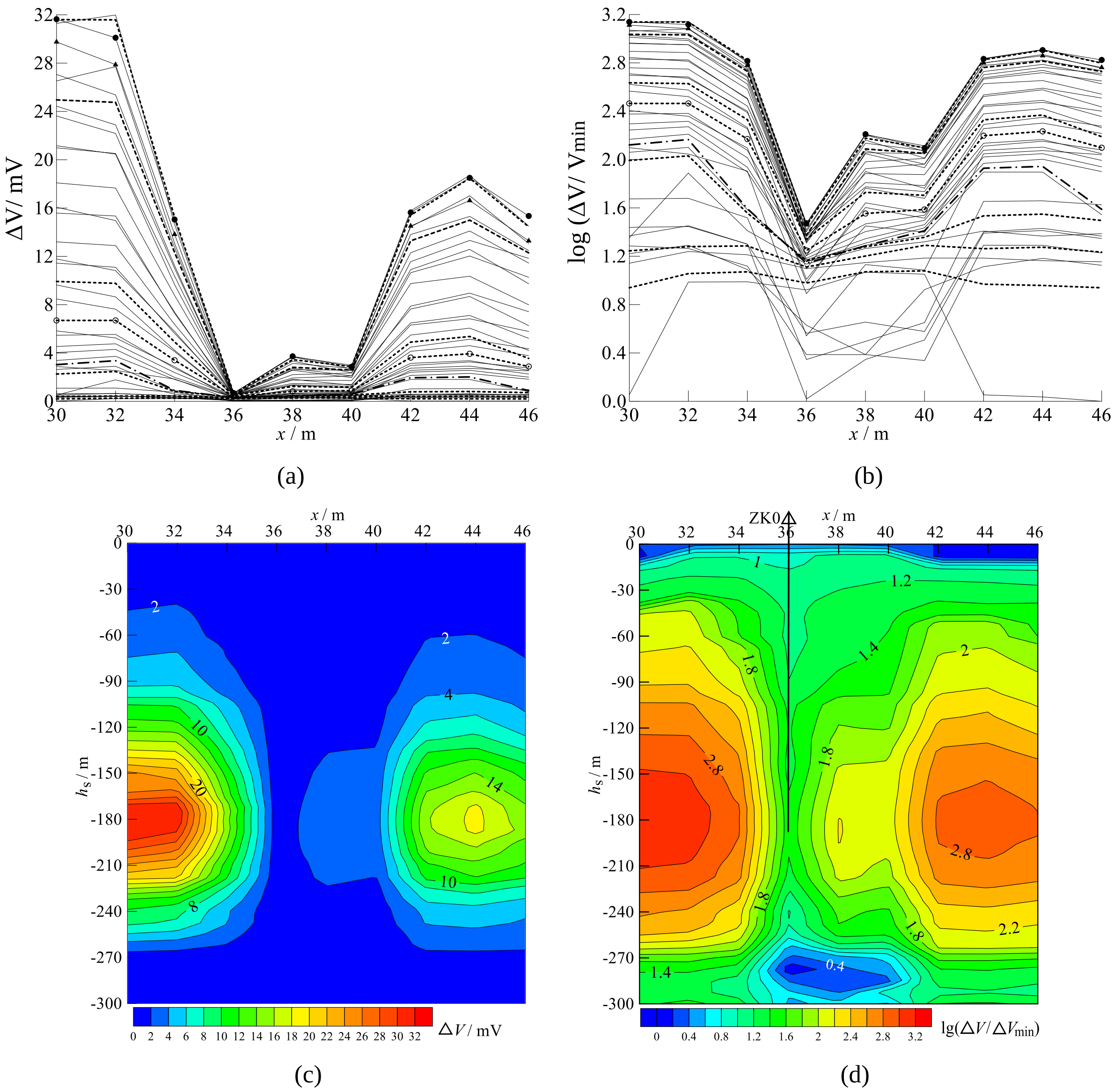

Figure 5. Profile curves and pseudo-sections of ΔV near 40 m of the profile in Lengshuijiang City. Profile curves (a) pre-processed and (b) post-processed, pseudo-sections (c) pre-processed and (d) post-processed by the logarithmic approach.

Figure 5(d) and Fig. 6(d) are pseudo-sections after logarithmic processing, and the center positions of the "noodles phenomenon" are more clearly. The spatial width of the relatively low-potential anomaly at 36 m in the pseudo section (Fig. 5) decreases from approximately 1 m (Fig. 5(c)) to a well-defined, clearly resolved anomaly center (Fig. 5(d)). Likewise, the width of the relatively low-potential anomaly at 80 m in Fig. 6 decreases from ~2.5 m (Fig. 6(c)) to ~1.8 m (Fig. 6(d)). We can see that the anomaly resolution in Fig. 5(d) and 6(d) is significantly better than those in Fig. 5(c) and 6(c). The drilling position ZK0 was selected at 36 m of the profile, represented as a triangle point in Fig. 5(d) based on the principle of static shift for water exploration ([6, 13]) and the influence of carbonaceous shale. Groundwater began to appear at 130-m depth. The discharge water was ca. 150 t/day drilled at depth of 188 m. There is no more drilling was carried out because the water requirement was met.

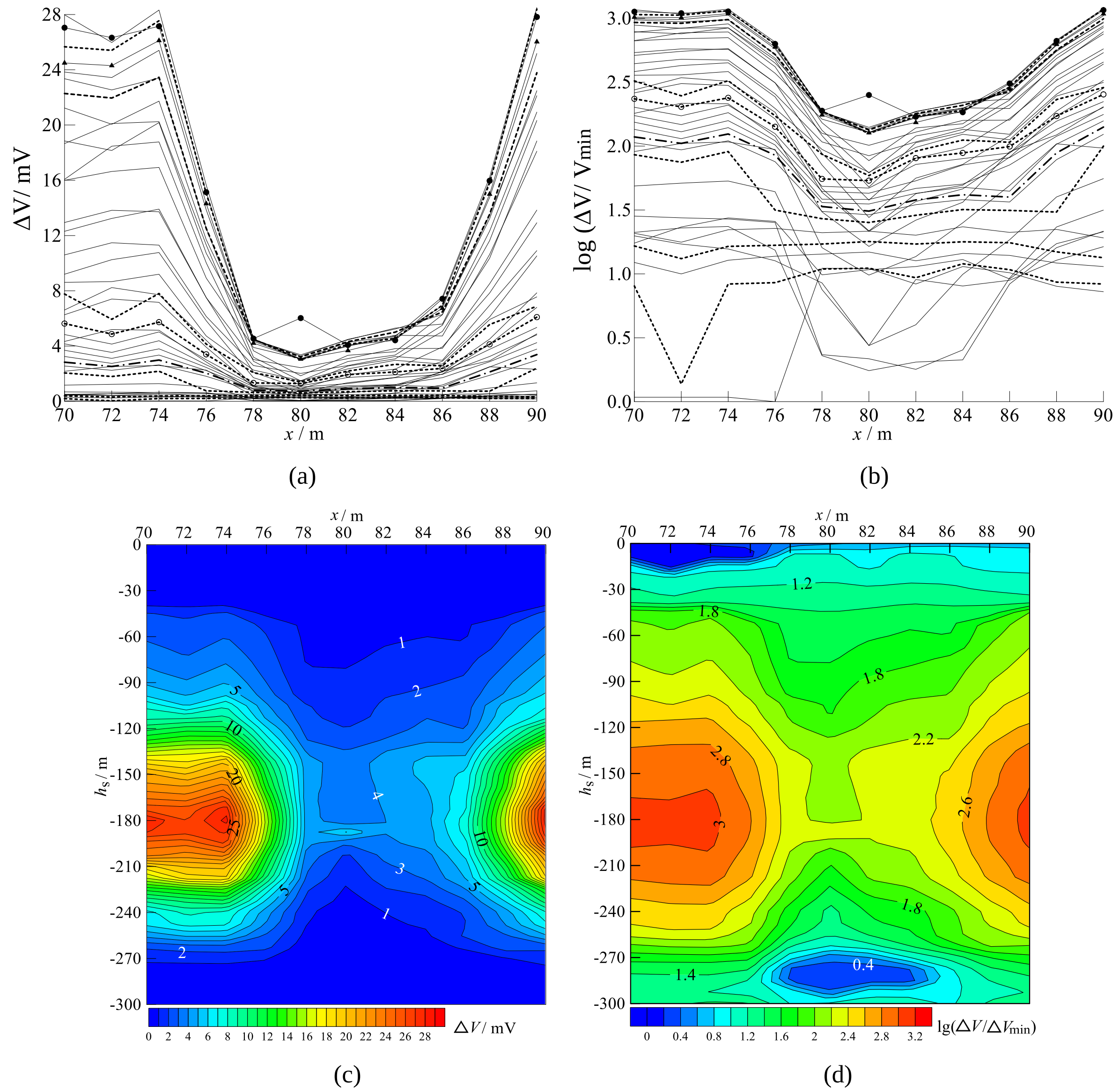

Figure 6. Profile curves and pseudo-sections of ΔV near 80 m of the profile in Lengshuijiang City. Profile curves (a) pre-processed and (b) post-processed, pseudo-sections (a) pre-processed and (b) post-processed by the logarithmic approach.

4.2 Groundwater Exploration in a Caledonian Granodiorite area

We still adopted a TC300 system, and electrode spacing (*MN*) and station intervals are 10 m and 5 m, respectively. Figure 6 shows the measured results with three frequencies of TEFSM for the mineral water detection at a farm (28º29'56.80"N, 112º3'58.51"E) of Taojiang County (Fig. 3), Hunan Province, China. The lithology of studied area is the late Caledonian granodiorite. The black dots in Fig. 7 represent low potential anomalies. Due to the most obvious anomaly at 130 m of the profile, we thought this was the most favorable location for water exploration.

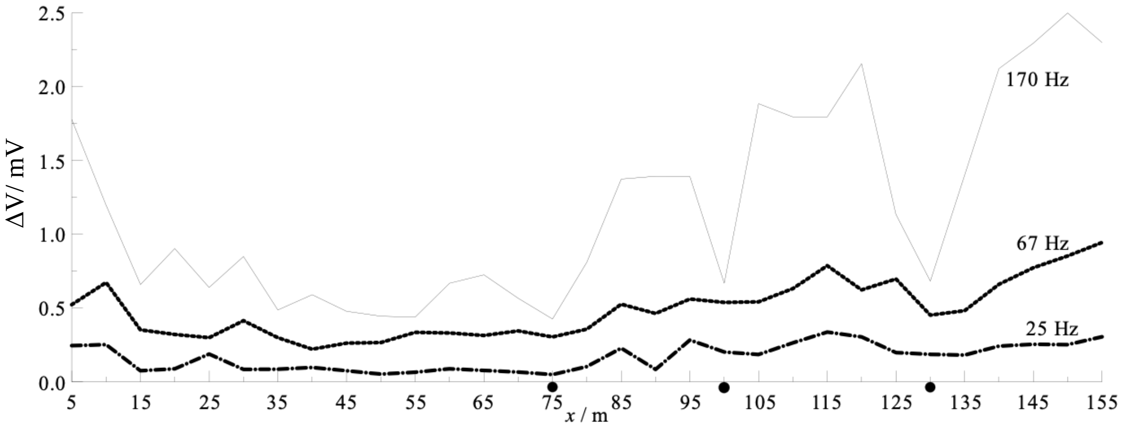

Figure 7. The TEFSM exploration results obtained with three frequencies long the profile in Taojiang County. The black dots indicate the positions of the anomalous body to be explored for groundwater.

Figure 8 shows further study by multifrequency observation with a TC300 frequency selector at the electrode spacing (*MN*) and the station interval of 10 m and 2 m, respectively. The sampling frequencies are 40 within the range of 12-5000 Hz. Figure 8(a) and Fig. 8(b) are profile curves of potential difference ΔV pre-processed and post processed, respectively. The observed values in Fig. 8(a) are much smaller than those in Fig. 5(a) and is about 10 times relation. In addition to the change in the geological environment, the authors think that the current detection site lies in the rural area far from the industrial area, and the observation results are less affected by industrial electromagnetic interference. The low potential anomaly is located within the range of 128～135 m on this profile, and the synchronization of different frequency curves is poor. In Figs. 8(a) and 8(b), the precise center position of the low value anomaly cannot be unambiguously determined. Moreover, the relative amplitude of this low-value anomaly changes—from approximately 1:3 before logarithmic processing to ~1.2:1.7 after processing.

According to Fig. 8(c), a relatively low potential anomaly area at about depth 60～180 m is located in about 126 ～136 m on the profile. In addition, the area of the anomaly is too large, and the details of the granite fracture zone are not clear. Therefore, we used a logarithmic processing approach to enhance the signal of the observed data, aiming to obtain the pseudo-section shown in Fig. 8(c), which clearly shows the non-uniformity of underground conductive media in low potential anomalous areas. Following data processing, the center positions of the low-value anomalies are predominantly confined to the range of 131.0–134.5 m. The drilling position ZK1 was selected at 133 m of the profile represented as a triangle point in Fig. 8(d). The drilled well at the recommended location and 210 m deep resulted in a mineral water flow rate of ca. 450 t/day clearly signifies the effect of the proposed approach.

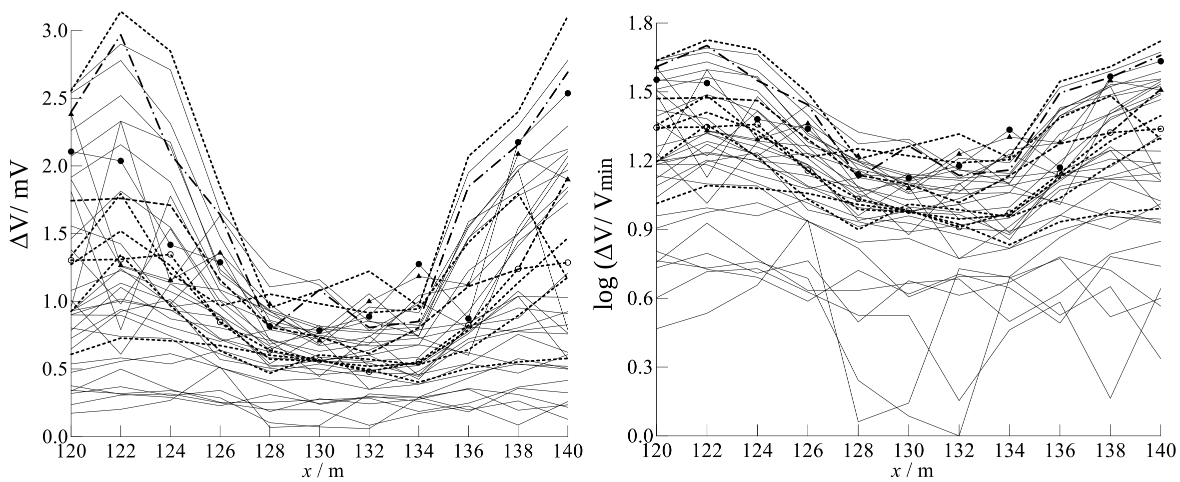

(a) (b)

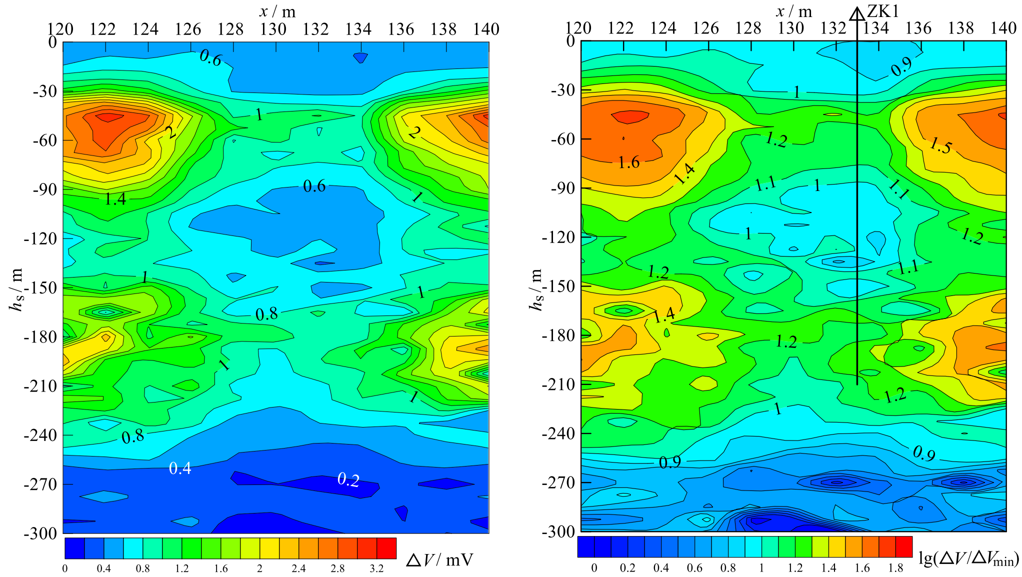

(c) (d)

Figure 8. Profile curves and pseudo-sections of ΔV near 130 m of the profile in Taojiang County. (a) Profile curves pre-processed and (b) post processed, pseudo-sections (c) pre-processed and (d) processed by the logarithmic approach.

4.3 Seepage Detection at a Reservoir Dam

Dishuiyan Reservoir is located in Zengjiaqiao Village, Lianhua Town, Xiangjiang New District, Changsha City, Hunan Province, China. It is classified as a small type II reservoir with a catchment area of 0.55 km^2 and a total storage capacity of 246600 m^2 (Fig. 9).

(a) (b)

Figure 9. (a) An aerial photograph; (b) a field photograph of Dishuiyan Reservoir

Due to significant seepage issues, the TEFSM was employed to identify potential leakage zones. The PQ-227B TEFSM dam piping detector was used, which measures 30 frequencies within the range of 450–5000 Hz at each station, achieving a detection depth of approximately 50 m. During field surveys, 26 electrodes were deployed simultaneously at 2.5 m intervals, enabling the synchronous acquisition of data from 22 observation stations. The electrode spacing (*MN*) for each station was set to 10 m. The red line with an arrow in Fig. 9(a) indicates the location and orientation of the survey line.

Figures 10(a) and 10(b) present the ΔV-profile curves and their logarithmically processed counterparts obtained position and direction of survey line from the TEFSM survey. As shown by the red dots in Fig. 10(a), distinct relatively low-potential anomalies are observed at 27.5 m, 35 m, 45 m, 57.5 m, 65 m, 87.5 m, 92.5 m, and 97.5–100 m along the survey line. These anomalies remain clearly identifiable after logarithmic processing (Fig. 10(b)). Additionally, a weaker low-potential anomaly is visible at 2.5 m. Based on the theoretical foundation of TEFSM anomaly generation and its established applications in groundwater detection, these anomalies suggest the presence of subsurface seepage beneath the corresponding locations.

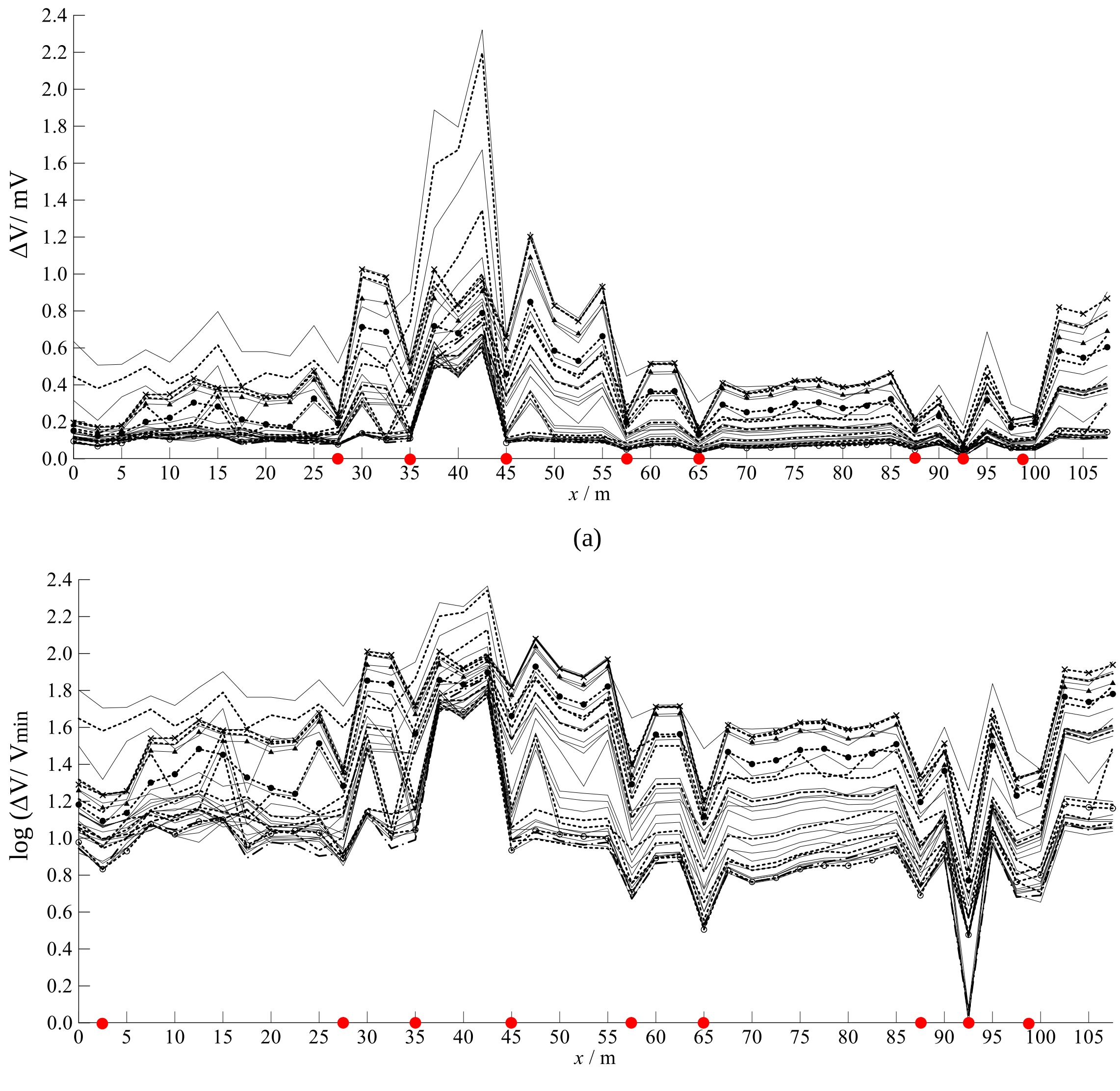

Figure 10. (a) ΔV profile curves from Dishuiyan Reservior; (b) logarithmically processed profile curves.

Figure 11 displays the ΔV pseudo-sections derived from depth inversion, with Fig. 11(a) and Fig. 11(b) showing results before and after logarithmic processing, respectively. In the depth range of approximately 7–27 m below the survey line, the measured ΔV values are predominantly below 0.1 mV, resulting in a uniformly blue representation in the pseudo-section (Fig. 11(a)). This indicates very low electrical resolution within this layer, making it difficult to determine the precise locations or depths of seepage pathways from the unprocessed data. In contrast, Fig. 11(b) shows the logarithmically normalized ΔV results, where contour lines in the 7–27 m depth range are denser and anomaly resolution is significantly enhanced. From this processed section, it can be inferred that severe seepage likely occurs between depths of 10–20 m at horizontal positions 57.5 m, 65 m, 70 m, 87.5 m, and 99 m, and between 10–30 m at 92.5 m. Minor seepage may also exist at 2.5 m and 27.5 m, at depths of approximately 13–22 m. Considering the spatial distribution and burial depths of these anomalous zones, it is reasonable to conclude that seepage in Dishuiyan Reservoir primarily occurs near the interface between the dam body and the underlying bedrock.

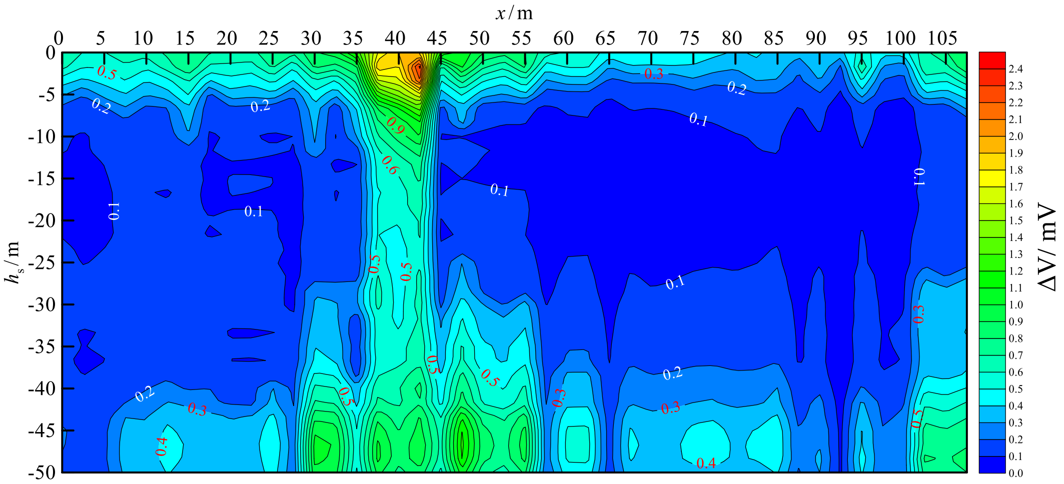

(a)

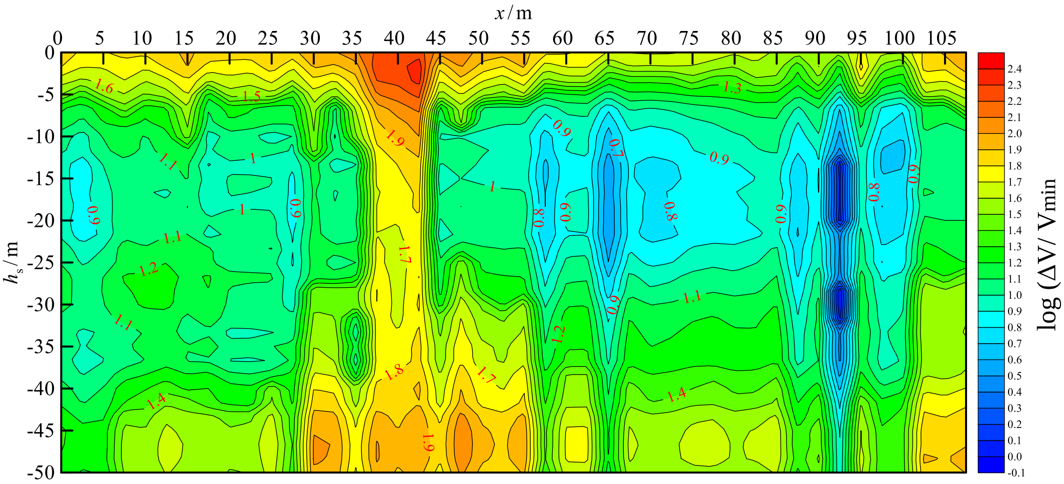

(b)

Figure 11. (a) ΔV pseudo-section of from Dishuiyan Reservior; (b) logarithmically processed pseudo-section.

5. CONCLUSIONS

In this paper, we presented a method to improve the resolution of TEFSM data through an efficient logarithmic processing approach. And this processing approach can be carried out immediately after in-field detection is completed. Data processing using this approach resulted in the enhancement of weak signals by compressing the raw signal range. The hypothesis is verified through its application on three case studies of societal significance, the groundwater exploration in quartz sandstone and granite settings, as well as the seepage detection at a reservoir dam. The method is simple and efficient in the sense that results can be obtained immediately for the rapid interpretation of field data. The adaption of the approach can potentially improve the resolution of observed data with better drilling accuracy through better detection of subsurface geological structures of interests. Notably, the data processing functionality has already been integrated into the newly developed frequency selector. Upon completion of on-site profile acquisition, users can perform full processing with a single click; the entire operation completes within 2 seconds.

Author Contributions

The first author and the second authors drafted the main body of the manuscript. The third author revised the manuscript and provided critical feedback. The fourth author contributed to data collection and processing. All authors reviewed and approved the final version of the manuscript.

Declaration of Competing Interest

The authors declare that they have no conflicts of interests.

Funding information

This article did not receive any funding, and this research work is mainly based on the authors’ interest.

REFERENCES

[1] Li Y, Wu Q, Wang S, Lei D, Yao D, Zhang Z, et al. Multi-channel observation experiments of audio-frequency magnetotelluric technology in shallow water. Journal of Applied Geophysics. 2021;184:104243. doi:10.1016/j.jappgeo.2020.104243

[2] Ren W, Ren Z, Xue G, Chen W, Zhao P, Liu J. Three-dimensional audio magnetotelluric imaging of the Yangyi geothermal field in Tibet, China. Journal of Applied Geophysics. 2023;211:104966. doi:10.1016/j.jappgeo.2023.104966

[3] Rathnayaka S, Gustafson CD, Yoxtheimer D, Nyblade A. Imaging freshwater and saline aquifers beneath Bradford County, Pennsylvania, USA, using Audio-Magnetotelluric (AMT) data. Journal of Applied Geophysics. 2024;220:105255. doi:10.1016/j.jappgeo.2023.105255

[4] Wang D, Yang T, Isah A, Qin Q, Zhu M. Theoretical analysis and application of the telluric electric field frequency selection method for shallow groundwater exploration. Frontiers in Earth Science. 2025;13. doi:10.3389/feart.2025.1705085

[5] Yang T, Xia D, Wang Q, Fu G. Theoretical research and application of frequency selection method for telluric electricity field. Central South University Press Changsha, China; 2017.

[6] Yang T, Hu F, Yu X, Fu G, Li J, Yang Z. Analysis and application of the responses of the frequency selection method of telluric electricity field. Geophysical and Geochemical Exploration. 2023;47(4):1010-7

[7] Yang T, Zhu D, Hussain Y, Huang R, Yu Q, Ding Q. Feasibility study of telluric magnetic field frequency selection method in groundwater exploration. Journal of Applied Geophysics. 2025;233:105608. doi:10.1016/j.jappgeo.2024.105608

[8] Yang T, Yang Z, Qin Q, Adagunodo TA, Zhu M. Simulation of the Telluric Electrical Field Frequency Selection Method and Its Application in Mineral Water Exploration. Water. 2025;17(22):3314. doi:10.3390/w17223314

[9] Melchinov VP, Pavlov AA. Experience with a Water Detector in the Study of the Permafrost Structure. Geomagnetism and Aeronomy. 2022;62(3):271-7. doi:10.1134/s0016793222030100

[10] Han R, Han D. Theory and practice of frequency selection method for telluric electricity field. Metallurgical industry press Beijing; 2020.

[11] Yang T, Chen Z, Liang J. Theoretical analysis of sounding anomaly and practical application of the frequency selection sounding method of natural electric field in groundwater exploration. Earth Science Frontiers (in Chinese). 2020;27(4):302-10

[12] Yang T, Wang D, Zhang Y, FU G, Chen B, Yang Z, et al. Application research of comprehensive geophysical method to karst investigation in a productive mine. Progress in Geophysics. 2021;36(3):1145-53

[13] Yang T, Gao Q, Li H, Fu G, Hussain Y. New Insights into the Anomaly Genesis of the Frequency Selection Method: Supported by Numerical Modeling and Case Studies. Pure and Applied Geophysics. 2023;180(3):969-82. doi:10.1007/s00024-022-03220-8

[14] Lu Y, Ding H, Yang T, Liu Y. Geothermal Water Exploration of the Maoyanhe Hot Spring Scenic Spot in Zhangjiajie Using the Natural Electric Field Frequency Selection Method. Water. 2023;15(19):3418. doi:10.3390/w15193418

[15] Yulong L, Tianchun Y, Tizro AT, Yang L. Fast Recognition on Shallow Groundwater and Anomaly Analysis Using Frequency Selection Sounding Method. Water. 2022;15(1):96. doi:10.3390/w15010096

[16] Abu El Ata AS, Nabawy BS, Badran OM. Integration of shallow geoelectrical investigations for delineating the hidden water springs, case study: Ayun Mousa, Northern Gulf of Suez, Egypt. Environmental Technology & Innovation. 2021;22:101499. doi:10.1016/j.eti.2021.101499

[17] Vinoth Kingston J, Antony Ravindran A, Richard Abishek S, Aswin SK, Antony Alosanai Promilton A. Integrated geophysical and geochemical assessment of submarine groundwater discharge in coastal terrace of Tiruchendur, Southern India. Applied Water Science. 2021;12(1). doi:10.1007/s13201-021-01553-8

[18] Lian K. Application of sound frequency geoelectric field method in detecting groundwater in karst mountainous areas. Hydrogeology & Engineering Geology. 1979;5:76-85

[19] Yang J. Experimental results and theoretical study of the stray current method in karst area. Geophys Geochem Explor. 1982;6(1):41-54

[20] Lin J, Lei C, Dong Q. The natural low frequency electric field method. Journal of Changchun University of Earth Sciences. 1983;13:114-26

[21] Chen S. Application of frequency selection method of telluric current in water prospecting. Geotechnical Investigation & Surveying. 1988;16(2):53-5

[22] Lian K, Zhu R, Guo J. Preliminary application of the audio geoelectric field method to the investigation of geological hazard. The Chinese Journal of Geological Hazard and Control. 1991;2:37-41

[23] Luo H. The coal palaeoadit disaster and it's forecast by the natural electric field method. The Chinese Journal of Geological Hazard and Control. 1994;5:277-84

[24] Song W, Li Z, Jin Y, Zhang B, Zheng T. Comprehensive application of hydrogeological survey and in-situ thermal response test. Case Studies in Thermal Engineering. 2021;27:101287. doi:10.1016/j.csite.2021.101287

[25] Adagunodo TA, Ojoawo AI, Anie NO, Edukugho PO. Application of frequency selection and geoelectrical sounding methods for mapping of leachate's pathways in an active dumpsite. SN Applied Sciences. 2023;5(12). doi:10.1007/s42452-023-05557-8

[26] Gomo M. Use of electric potential difference in audio magnetotelluric (AMT) geophysics for groundwater exploration. Groundwater for Sustainable Development. 2023;20:100864. doi:10.1016/j.gsd.2022.100864

[27] Alabi AA, Popoola OI, Olurin OT, Ogungbe AS, Ogunkoya OA, Okediji SO. Assessment of groundwater potential and quality using geophysical and physicochemical methods in the basement terrain of Southwestern, Nigeria. Environmental Earth Sciences. 2020;79(14). doi:10.1007/s12665-020-09107-y

[28] Zonge KL, Sauck WA, Sumner JS. Comparison of Time, Frequency, and Phase Measurements In Induced Polarization. Geophysical Prospecting. 1972;20(3):626-48. doi:10.1111/j.1365-2478.1972.tb00658.x

[29] Li J, Zhang X, Tang J. Noise suppression for magnetotelluric using variational mode decomposition and detrended fluctuation analysis. Journal of Applied Geophysics. 2020;180:104127. doi:10.1016/j.jappgeo.2020.104127

[30] Xie J, Cai H, Hu X, Long Z, Xu S, Fu C, et al. 3-D Magnetotelluric Inversion and Application Using the Edge-Based Finite Element With Hexahedral Mesh. IEEE Transactions on Geoscience and Remote Sensing. 2022;60:1-11. doi:10.1109/tgrs.2021.3079420

[31] Xie J, Cai H, Ren B, Yang T, Liao J, Cao S, et al. 3-D Adaptive Multinary Inversion of Magnetotelluric Data Using Unstructured Tetrahedral Mesh. IEEE Transactions on Geoscience and Remote Sensing. 2025;63:1-11. doi:10.1109/tgrs.2024.3517633

[32] Jones AG. Static shift of magnetotelluric data and its removal in a sedimentary basin environment. Geophysics. 1988;53(7):967-78. doi:10.1190/1.1442533

[33] Ogawa Y, Uchida T. A two-dimensional magnetotelluric inversion assuming Gaussian static shift. Geophysical Journal International. 1996;126(1):69-76. doi:10.1111/j.1365-246x.1996.tb05267.x

[34] Berdichevsky MN, Dmitriev VI. Models and Methods of Magnetotellurics. Springer Berlin Heidelberg; 2008.

[35] Yu S-B, Zheng J-B, Gao M-L, Luan H. CSAMT static correction method based on wavelet transform modulus maxima and thresholds. Chinese Journal of Geophysics. 2017;60(1):360-8

[36] Tang J, He J. Controlled source audio-frequency Magnetotellurics and Applications. Changsha: Central South University Press; 2005.

[37] Lei D, Fayemi B, Yang L, Meng X. The non-static effect of near-surface inhomogeneity on CSAMT data. Journal of Applied Geophysics. 2017;139:306-15. doi:10.1016/j.jappgeo.2017.03.003

[38] Hu J, Motagh M, Wang J, Qin F, Zhang J, Wu W, et al. Karst Collapse Risk Zonation and Evaluation in Wuhan, China Based on Analytic Hierarchy Process, Logistic Regression, and InSAR Angular Distortion Approaches. Remote Sensing. 2021;13(24):5063. doi:10.3390/rs13245063

[39] Ward SH. Electromagnetic theory for geophysical applications. Mining Geophysics Volume-II: Theory. 1967

[40] Wang Z, Liu Y, Du J, Wang Z, Shao Q. De-noising magnetotelluric data using variational mode decomposition combined with mathematical morphology filtering and wavelet thresholding. Journal of Applied Geophysics. 2022;204:104751. doi:10.1016/j.jappgeo.2022.104751

[41] Chen H, Yu N, Kong W, Wang F, Li T. A stable analytical expression for magnetotelluric/radiomagnetotelluric impedances in anisotropic layered Earth models. Journal of Applied Geophysics. 2023;217:105184. doi:10.1016/j.jappgeo.2023.105184

[42] Yu G, Lei T, Zhang W, Chen X, He Z. Joint inversion of two-dimensional magnetotelluric and ambient noise data constrained with cross gradient. Journal of Applied Geophysics. 2023;215:105085. doi:10.1016/j.jappgeo.2023.105085

[43] Wang Z, Li Z, Liu Y, Peng J, Long S, Mills J. A New Processing Chain for Real-Time Ground-Based SAR (RT-GBSAR) Deformation Monitoring. Remote Sensing. 2019;11(20):2437. doi:10.3390/rs11202437

[44] Hu F, Yang T, Adagunodo TA, Zhu D, Huang R. Practice and theoretical analysis of ground penetrating radar in voids detection of urban underground pipe-jacking. Journal of Applied Geophysics. 2025;233:105639. doi:10.1016/j.jappgeo.2025.105639

[45] Tianchun Y, Debing Z, Guohong F, Zhui Y, Rui H. Shallow groundwater exploration by frequency selection method of telluric current in interference environment of high voltage transmission lines. China Sciencepaper. 2024;19(10)

